



Reflective color filters deposited via ZnS single-target sputtering for colorful solar cell applications

Dae-Hyung Cho^{a,b,*}, Woo-Jung Lee^{a,b}, Tae-Ha Hwang^a, Yong-Duck Chung^{a,b,**}

^a Superintelligence Creative Research Laboratory, Electronics and Telecommunications Research Institute (ETRI), Daejeon, 34129, Republic of Korea

^b Department of Advanced Materials and Device Engineering, Korea University of Science and Technology (UST), Daejeon, 34113, Republic of Korea

ARTICLE INFO

Handling Editor: Dr P. Vincenzini

Keywords:

ZnS
Zn(O,S)
Color filter
Sputtering
Thin film solar cell

ABSTRACT

The use of colorful solar cells is necessary for building-integrated photovoltaic (BIPV) applications in urban areas, where aesthetics play an important role. The conventional deposition process of multilayer color filters utilized in solar cells for BIPV applications is expensive because it requires multiple sputter targets. Herein, to address the issue of high cost, a single sputter target was used to produce a color filter consisting of a Zn-based multilayer structure. The oxygen content in the Zn(O,S) films could be controlled by adjusting the amount of oxygen gas supplied during the sputtering process. This allows for control of the optical properties of the films, including the refractive index and extinction coefficient. A color filter with the Zn(O_{0.92}S_{0.08})/ZnS structure repeated three times was applied to Cu(In,Ga)Se₂ thin-film solar cells; the resulting solar cell demonstrated a wide range of color expressions and less than 10% reduction in optical performance. The proposed technology is expected to significantly reduce the cost of optical filter processes and their applications.

1. Introduction

In recent times, there has been a growing demand for the incorporation of color in devices such as solar cells, displays, mobile phones, and defense systems. Although improving photovoltaic performance remains a key priority, the development of technology that implements color to offer effective camouflage and provide visual and psychological enjoyment to humans is underway. In particular, the demand for colorization technology in photovoltaic applications has significantly increased. Conventional photovoltaic modules are dominated by monochromatic panels that only consider the power generation performance; however, of late, solar modules with different colors and various sizes and shapes have found applications in buildings in response to the demand for building-integrated photovoltaics (BIPVs) to support energy self-sufficiency in urban areas [1–8].

Multilayer optical interference filters are a common technology used in various devices to achieve low or high reflection in the desired wavelength range. Multilayer optical notch filters with layered interference coatings are widely used for color implementation [9–13]. An alternating formation of oxide-based high-refractive-index and

low-refractive-index films can be used to achieve constructive interference at specific wavelengths to produce reflection or transmission, enabling the realization of desired colors. The refractive index (*n*), thickness, and number of layers of the thin film can be adjusted to control the color. For use in colorful photovoltaic modules, a multilayer interference coating is commonly formed on a glass substrate and placed on the photovoltaic module. Color filters consist of high-refractive-index materials such as Al₂O₃, Nb₂O₅, and TiO₂, and low-refractive-index materials such as SiO₂ and MgF₂, which are deposited via sputtering or electron beam evaporation [11,14–16]. Sputtering, which is advantageous for large-area deposition, is the most widely used method for the mass production of color filters and photovoltaic applications [17–22]. However, forming a multilayer coating of different materials using sputtering requires different sputter targets for each material, which requires alternating depositions and results in increased deposition time and cost. In addition, the deposition process should be designed by considering the target arrangement and substrate transfer speed according to the thickness and number of layers.

If two or more types of thin films can be formed using a single target, the process cost can be considerably reduced by resizing the equipment

* Corresponding author. Superintelligence Creative Research Laboratory, Electronics and Telecommunications Research Institute (ETRI), Daejeon, 34129, Republic of Korea.

** Corresponding author. Superintelligence Creative Research Laboratory, Electronics and Telecommunications Research Institute (ETRI), Daejeon, 34129, Republic of Korea.

E-mail addresses: dhcho@etri.re.kr (D.-H. Cho), ydchung@etri.re.kr (Y.-D. Chung).

<https://doi.org/10.1016/j.ceramint.2023.07.010>

Received 29 March 2023; Received in revised form 2 July 2023; Accepted 3 July 2023

Available online 5 July 2023

0272-8842/© 2023 Elsevier Ltd and Techna Group S.r.l. All rights reserved.

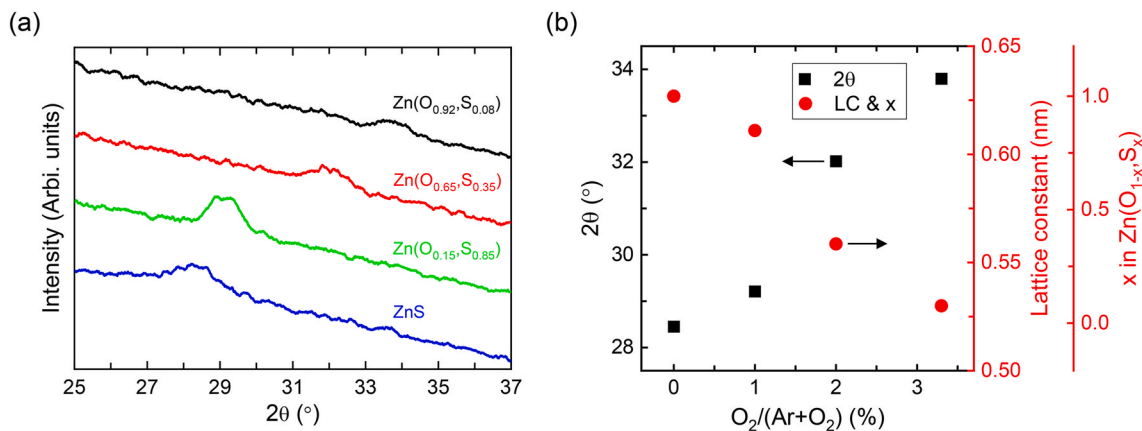


Fig. 1. (a) XRD results of Zn(O,S) thin films with different $O_2/(Ar + O_2)$ ratios and their (b) lattice constants and S-to-O composition ratios estimated from the 2θ values.

and vacuum chambers, including the sputter guns, and the yield can be increased.

In this study, we propose a method for fabricating a color filter using only a single ZnS target. The refractive index of the Zn(O,S) thin film was controlled by changing the oxygen content and controlling the O_2 gas supply during sputtering. The single-target-based color filter was manufactured by stacking thin films with different refractive indices, thereby reducing production cost and facilitating process engineering according to the change in the structure. Furthermore, we analyze the structural and optical properties of Zn(O,S) thin films and the optical and electrical performance of the solar cells with the color filters applied.

2. Material and methods

Zn(O_{1-x}S_x) thin films were deposited via radio frequency (RF) magnetron sputtering using a single ZnS target. The details of the sputter system and the mechanism of thin film formation are described in our previous papers [23,24]. By adjusting the O_2 gas flow ratio ($O_2/(Ar + O_2)$) at 3.3%, 2.0%, 1.0%, and 0%, S-to-O composition ratios (x , S/(O + S)) of 0.08, 0.35, 0.85, and 1.00 were obtained in the Zn(O_{1-x}S_x) thin films, respectively. The total gas flow rate under each condition was 61 sccm, and the O_2 :Ar flow rates were 2.0:59.0, 1.2:59.8, 0.6:60.4, and 0:61 under the four O_2 gas flow ratios of 3.3%, 2.0%, 1.0%, and 0%, respectively [25]. The total pressure during deposition was 4 mTorr and the substrate temperature was 185 °C; the RF power was maintained at 150 W. The diameter of the ZnS target was 10.16 cm.

The color filter consisted of six layers formed by alternating depositions of the Zn(O_{0.92}S_{0.08}) and ZnS thin films three times each. The deposition rates of the Zn(O_{0.92}S_{0.08}) and ZnS thin films were 0.552 and 1.284 Å/s, respectively.

A Cu(In,Ga)Se₂ (CIGS) thin-film solar cell was fabricated with Al/Ni/indium tin oxide (ITO)/ZnO/Zn(O,S)/CIGS/Mo/soda-lime glass structure using the baseline process described in previous studies [13,26–30]. First, a 900-nm-thick Mo rear electrode was deposited on a 1.1-mm-thick soda-lime glass substrate via direct current sputtering. Subsequently, a CIGS absorber layer was formed using a co-evaporation method in which Cu, In, Ga, and Se were independently evaporated. The evaporated elements in each stage changed in the following order: In-Ga-Se, Cu-Se, and In-Ga-Se. A Zn(O,S) buffer layer was synthesized via chemical bath deposition using an aqueous solution of thiourea, NH₄OH, and ZnSO₄ [31–33]. A resistive layer of ZnO and a transparent ITO electrode were deposited with thicknesses of 70 and 150 nm, respectively, through RF sputtering. Finally, for the metal grid contact, Ni and Al were formed with thicknesses of 50 nm and 3 μm, respectively, by electron beam evaporation.

The thickness of each layer in the color filter was determined via

computer simulation using Essential Macleod software (Thin Film Center Inc.) to achieve the target color. The measured optical characteristics of the solar cells and the refractive indices and extinction coefficients (k) of the Zn(O_{0.92}S_{0.08}) and ZnS thin films were used the simulation. The reflectance/transmittance spectra and color parameters of the designed filters were also obtained via computer simulations.

The structural properties of the fabricated Zn(O,S) thin films were analyzed via X-ray diffraction (XRD) 2θ - ω measurements (X'pert PRO-MPD, Malvern Panalytical Ltd., UK). The light transmittance and reflectance of the thin films were measured using a UV-VIS spectrophotometer (Lambda 950, PerkinElmer, USA) [34]. The thicknesses, refractive indices, and extinction coefficients of the thin films were measured using a spectroscopic ellipsometer (M200D (RCT), JA Woolam, USA). The external quantum efficiency (EQE) was measured using spectrally resolved monochromatic light generated by a 12 W halogen lamp (Newport, USA). The optical performance of the solar cell was analyzed by measuring the current density (J) and voltage (V) using a current-voltage source meter (Keithley 2400, Keithley Instruments, USA) under 1 kWm⁻² irradiance by an Air Mass 1.5G Spectrum; the short-circuit current density (J_{SC}) was then obtained from a plot of J - V curve. The grid pads were protected from color-filter deposition to facilitate electrical contact. The samples were light-soaked under solar irradiation for 1 h to achieve a performance-saturated state before measuring the J - V and EQE [31,33].

3. Results and discussion

We observed the change in the S-to-O composition ratio with respect to the amount of O_2 supplied and the corresponding changes in the structural properties of the Zn(O,S) thin films. The XRD results shown in Fig. 1(a) indicated that a (0002) peak was observed in all Zn(O_{1-x}S_x) thin films at different positions depending on the value of x . Fig. 1(b) shows a plot of the 2θ value of the (0002) peak, the lattice constant (LC), and the S-to-O composition ratio as a function of the O_2 gas flow ratio. At O_2 gas flow ratios of 3.3%, 2.0%, 1.0%, and 0%, the 2θ values were 33.80°, 32.02°, 29.21°, and 28.45°, respectively. The thicknesses of the thin films were 37, 39, 62, and 86 nm, respectively, and the LC values calculated using Bragg's law were 0.530, 0.559, 0.611, and 0.627 nm, respectively. The x value in Zn(O_{1-x}S_x) and LC have a strong linear relationship that satisfies Vegard's rule and is empirically expressed as follows [35,36]:

$$x = (9.01 \times LC \text{ [nm]}) - 0.518 \quad (1)$$

Thus, the S-to-O composition ratio x was found to be 0.08, 0.35, 0.85, and 1.00 in samples with O_2 gas flow ratios of 3.3%, 2.0%, 1.0%, and 0%, respectively. The S-to-O composition ratio in the Zn(O,S) thin films

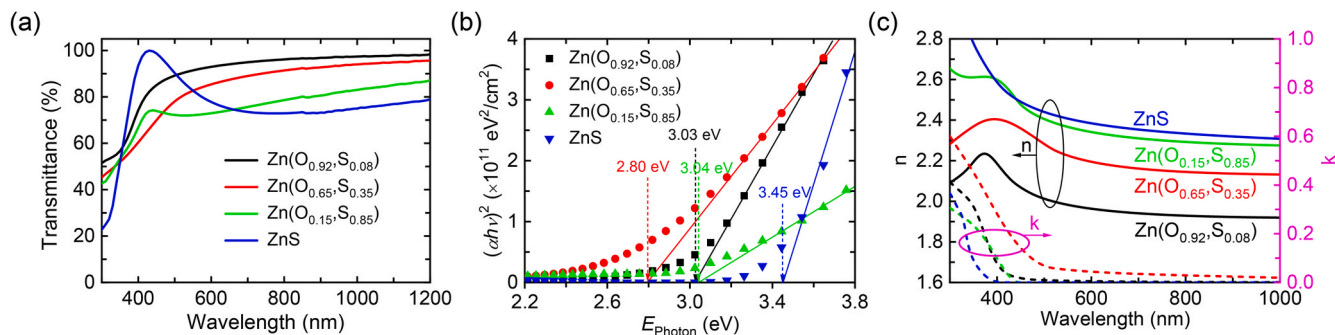


Fig. 2. (a) Transmittance, (b) Tauc plot, and (c) refractive index and extinction coefficient of Zn(O,S) thin films with different S-to-O composition ratios.

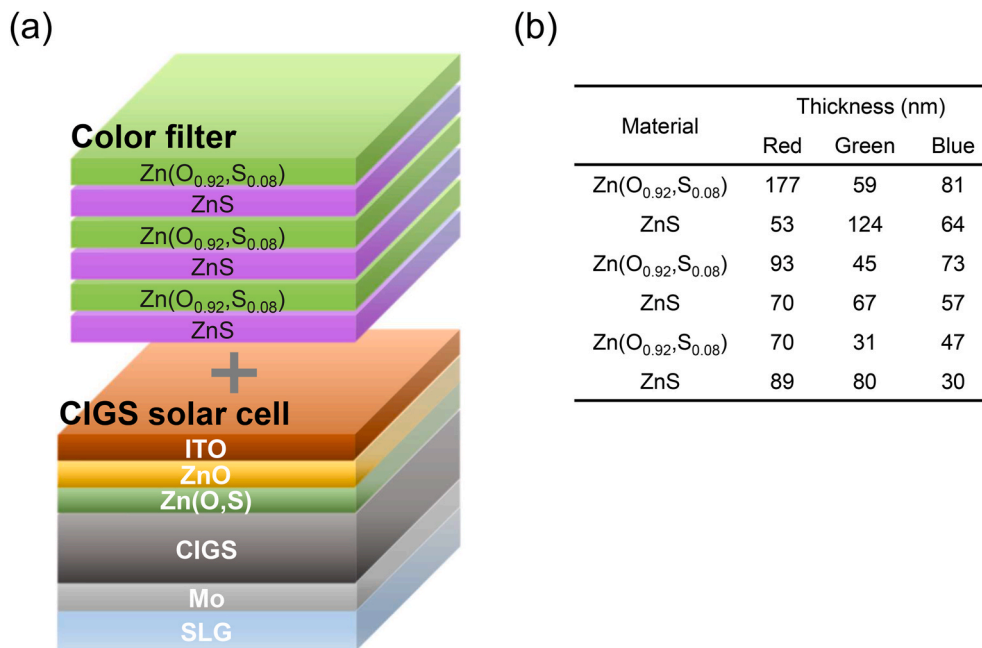


Fig. 3. (a) Schematic of the color-filter-applied CIGS solar cell structure and (b) designed thickness of each layer for red, green, and blue reflective color. (For interpretation of the references to color in this figure legend, the reader is referred to the Web version of this article.)

could be precisely and easily controlled over a wide range by controlling a small amount of the incorporated O₂ gas.

The optical characteristics of the Zn(O,S) thin films according to the S-to-O composition ratio were analyzed, and the color filter layer conditions capable of maintaining vivid color and adequate solar cell performance were explored. Fig. 2(a) and (b) display the transmittances and their Tauc plots for the Zn(O_{0.92}S_{0.08}), Zn(O_{0.65}S_{0.35}), Zn(O_{0.15}S_{0.85}), and ZnS thin films, which show bandgap energies (*E_g*) of 3.03, 2.80, 3.04, and 3.45 eV, respectively, with high transmittances in the visible wavelength region. The *E_g* of Zn(O,S) shows a bowing pattern wherein the *E_g* initially decreases and subsequently increases with an increase in the S-to-O composition ratio is expressed as follows [37–40]:

$$E_{g,Zn(O_{1-x}S_x)} = xE_{g,ZnS} + (1-x)E_{g,ZnO} - bx(1-x) \quad (2)$$

We confirmed that the bowing factor (*b*) was 2.1 eV in the Zn(O,S) thin film fabricated in our previous study [23,24]. The bandgap obtained from the Tauc plot in Fig. 2(b) satisfies this relationship. The optical properties of the color filter that can simultaneously satisfy solar cell application and color implementation were observed. Fig. 2(c) shows the refractive index (*n*) and extinction coefficient (*k*) as functions of the wavelength measured by a spectroscopic ellipsometer. Differences were observed in the refractive index and extinction coefficient of the thin films. As the S-to-O composition ratio increased, *n* increased over

the entire visible light wavelength range. The *n* values at a wavelength of 600 nm were 1.96, 2.19, 2.34, and 2.38 at *x* = 0.08, 0.35, 0.85, and 1.00, respectively, which is similar to the reported values [41,42]. The *k* values were negligible for wavelengths longer than 500 nm, whereas a large difference was observed for wavelengths shorter than 500 nm [39]. The smaller the *E_g* obtained in Fig. 2(b), the larger the *k* in the short-wavelength region. The *k* values at a wavelength of 400 nm were 0.079, 0.282, 0.099, and 0.003 at *x* = 0.08, 0.35, 0.85, and 1.00, respectively.

As the difference in the refractive index increases, more vivid colors can be realized in a color filter via a multilayer structure consisting of thin films with high and low refractive indices. For the implementation of a color filter in a solar cell, a smaller extinction coefficient in the wavelength range used for photoelectric conversion is more advantageous for optical gain. Therefore, in this study, Zn(O_{0.92}S_{0.08}) and ZnS which have the largest difference in refractive index and relatively small extinction coefficients in the short-wavelength regions were chosen for the fabrication of color filters.

The color filters were deposited on the top of the fabricated CIGS solar cells. Fig. 3 shows a (a) schematic of the structure of the CIGS solar cell and the color filter fabricated on it and (b) the thickness of each layer of the color filter for red, green, and blue color implementations. The color filter was fabricated with a structure in which the ZnS/Zn

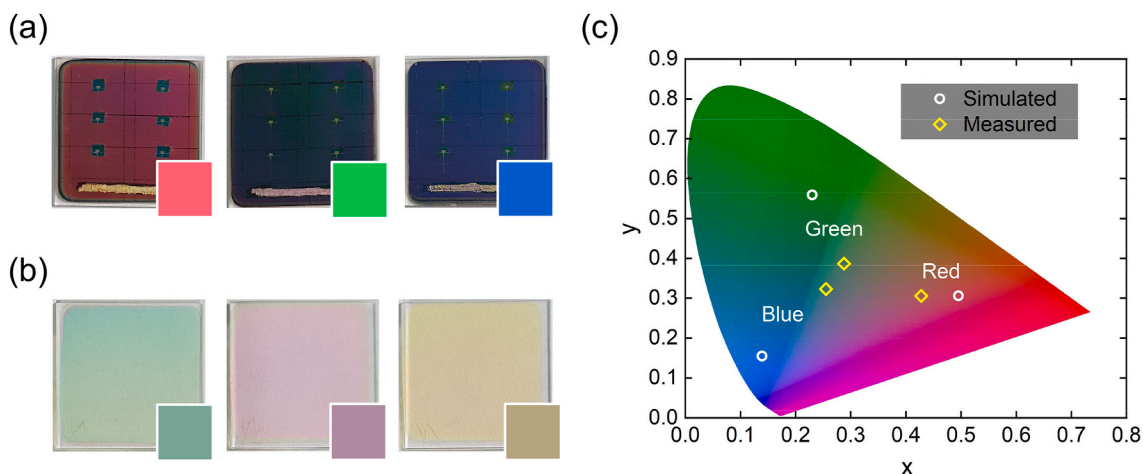


Fig. 4. Photographs of the red (left), green (center), and blue (right) color filters fabricated on the (a) solar cells and (b) glass substrates. The inset color patches indicate the simulated color. (c) Corresponding simulated and measured color coordinates of the solar cell samples plotted on a CIE 1931 xyY color space at $Y = 0.15$. (For interpretation of the references to color in this figure legend, the reader is referred to the Web version of this article.)

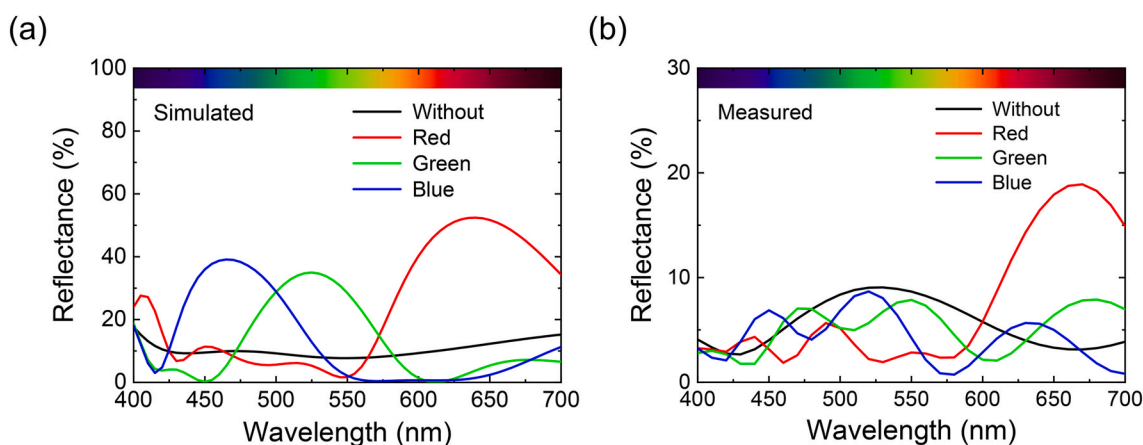


Fig. 5. Simulated and measured reflectance values of the solar cells with red, green, and blue color filters. (For interpretation of the references to color in this figure legend, the reader is referred to the Web version of this article.)

($O_{0.92}$, $S_{0.08}$) layer was repeated three times. The thickness of each layer was determined through computer simulations to realize red, green, and blue colors, and the total thicknesses were 552, 406, and 350 nm, respectively.

The color performances of the color filters were analyzed. Fig. 4(a) and (b) show photographs of the red, green, and blue color filters fabricated on the solar cell and glass substrate and their simulation results (inset color patch). Fig. 4(c) shows the measured values and simulation results of the xy color index. The color filters on the glass substrates in Fig. 4(b) are transmissive colors photographed on a white background, which are very similar to the colors obtained from the simulation results. Therefore, the target thickness and composition of the layered structure of the thin film were achieved. As shown in Fig. 4(a), the sample with color filters on the solar cells was also well-implemented for the three colors. The (x, y, Y) color index values of the red, green, and blue samples were (0.428, 0.305, 4.21), (0.288, 0.387, 5.61), and (0.255, 0.323, 4.49), respectively (Fig. 4(c)). However, the sample with the color filter formed on the solar cell was darker than the simulated sample and exhibited a narrower color range in the color coordinates. Because the CIGS solar cell was not completely black, the color obtained was slightly different from that obtained in the simulation result. In addition, in the case of the solar cell sample, light scattering occurred on the surface because of the high roughness resulting from the stacking of several layers of compound thin films. The surface

root-mean-square roughness of CIGS solar cells is known to reach up to 200 nm [43,44]. The simulation results (a) and measurement results (b) for the reflectance of the solar cell with the color filter applied are displayed in Fig. 5. In the simulation, the solar cell with the color filter was designed to have peaks at 640, 525, and 465 nm for red, green, and blue light, respectively. However, peak shifts and secondary peaks were observed in the measured samples because the broad reflectance peak at approximately 530 nm observed on the surface of the solar cell without a color filter influenced the background reflectance, and the surface roughness lowered the reflectance intensity.

The spectral optical gains of the solar cells with each color filter were measured in order to confirm the availability of the color filter for the solar cell application. Fig. 6 shows the EQE results for the (a) red, (b) green, and (c) blue solar cells. The EQE was measured before and after color filter deposition for the cells with the highest J_{SC} among the six cells of each sample. Relatively low EQE values were obtained in the wavelength range with high reflectance, in agreement with the reflectance results shown in Fig. 5(b). Fig. 6(d) shows the J_{SC} performance of the six cells of each sample before and after color filter formation. The average J_{SC} value of the red solar cell decreased by 3.39 mA/cm^2 (9.9%) from 34.12 mA/cm^2 to 30.73 mA/cm^2 after color filter deposition. The J_{SC} value of the green sample decreased by 2.15 mA/cm^2 (6.3%) from 34.11 mA/cm^2 to 31.96 mA/cm^2 , and that of the blue sample decreased by 2.13 mA/cm^2 (6.3%) from 33.73 mA/cm^2 to 31.60 mA/cm^2 . To

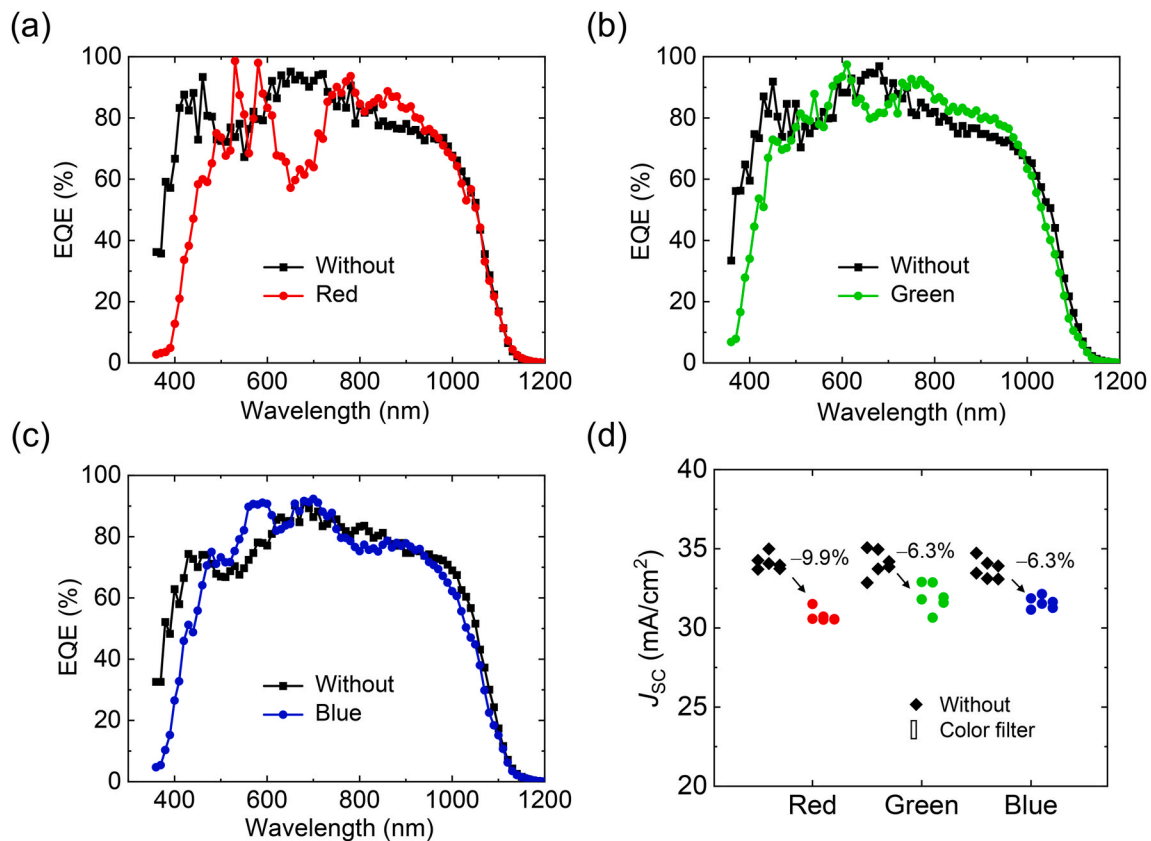


Fig. 6. EQE results of the solar cells before and after coating with the (a) red, (b) green, and (c) blue color filters. (d) The J_{sc} values of the solar cells with and without color filters. (For interpretation of the references to color in this figure legend, the reader is referred to the Web version of this article.)

maintain electrical contact for electrical performance measurement of the solar cells, Kapton® tape was attached to the metal contact pad before the color filter deposition, and the tape was removed after deposition. During this process, the metal grid was damaged, causing a significant decrease in the fill factor owing to an increase in the series resistance. However, it appears that this problem caused by the in-house process can be resolved if a color-filter-deposited solar cell is mass-produced.

4. Conclusions

We fabricated a color filter by alternately depositing thin films with different refractive indices to achieve an appropriate thickness using a single ZnS sputter target. This approach helps fabricate solar cells with various colors and minimal performance degradation. The refractive index and extinction coefficient were controlled by adjusting the oxygen content of the Zn(O,S) thin film, which was achieved by varying the O₂ gas flow rate during sputtering. Highly efficient CIGS thin-film solar cells of various colors such as red, green, and blue, were fabricated by selecting thin films with an S-to-O composition ratio that offers both a large refractive index difference and a low extinction coefficient. This fabrication process led to a wide range of color expression and a small reduction in J_{sc} performance, ranging from 6.3% to 9.9% depending on the color. Optimization of the thickness and number of layers in the color filter structure is expected to result in a wider range of colors and minimize the degradation in solar cell performance. The technology proposed herein, which requires only a single ZnS target and adjustable O₂ gas flow rate, can contribute to significantly reducing the production cost of color filters for solar cells.

Declaration of competing interest

The authors declare that they have no known competing financial interests or personal relationships that could have appeared to influence the work reported in this paper.

Acknowledgments

This work was supported by the program of Phased development of carbon neutral technologies through the National Research Foundation of Korea (NRF) funded by the Ministry of Science, ICT & Future Planning [grant number 2022M3J1A1063019] and by an Electronics and Telecommunications Research Institute (ETRI) grant funded by the Korean government [grant number 22YB1510].

References

- [1] J. Palm, L. Tautenhahn, J. Weick, R. Kalio, J. Kullmann, A. Heiland, S. Grönstedt, N. Schmidt, P. Borowski, F. Karg, BIPV modules: critical requirements and customization in manufacturing, in: 7th World Conference on Photovoltaic Energy Conversion (WCPEC) (A Joint Conference of 45th IEEE PVSC, 28th PVSEC & 34th EU PVSEC), IEEE Publications, 2018, pp. 2561–2566, <https://doi.org/10.1109/PVSC.2018.8547306>.
- [2] C. Ballif, L.-E. Perret-Aebi, S. Lufkin, E. Rey, Integrated thinking for photovoltaics in buildings, *Nat. Energy* 3 (2018) 438–442, <https://doi.org/10.1038/s41560-018-0176-2>.
- [3] A. Taşer, B.K. Koyunbaba, T. Kazanasmaz, Thermal, daylight, and energy potential of building-integrated photovoltaic (BIPV) systems: a comprehensive review of effects and developments, *Sol. Energy* 251 (2023) 171–196, <https://doi.org/10.1016/j.solener.2022.12.039>.
- [4] N. Skandalos, M. Wang, V. Kapsalis, D. D'Agostino, D. Parker, S.S. Bhuvad, Udayraj, J. Peng, D. Karamanis, Building PV integration according to regional climate conditions: BIPV regional adaptability extending Köppen-Geiger climate classification against urban and climate-related temperature increases, *Renew. Sustain. Energy Rev.* 169 (2022), 112950, <https://doi.org/10.1016/j.rser.2022.112950>.

- [5] N. Martín-Chivelet, K. Kapsis, H.R. Wilson, V. Delisle, R. Yang, L. Olivieri, J. Polo, J. Eisenlohr, B. Roy, L. Maturi, G. Otnes, M. Dallapiccola, W.M.P. Upalakshi Wijeratne, Building-Integrated Photovoltaic (BIPV) products and systems: a review of energy-related behavior, *Energy Build.* 262 (2022), 111998, <https://doi.org/10.1016/j.enbuild.2022.111998>.
- [6] T.M. Koh, H. Wang, Y.F. Ng, A. Bruno, S. Mhaisalkar, N. Mathews, Halide perovskite solar cells for building integrated photovoltaics: transforming building Façades into power generators, *Adv. Mater.* 34 (2022), 2104661, <https://doi.org/10.1002/adma.202104661>.
- [7] J. Bing, L.G. Caro, H.P. Talathi, N.L. Chang, D.R. McKenzie, A.W.Y. Ho-Baillie, Perovskite solar cells for building integrated photovoltaics—glazing applications, *Joule* 6 (2022) 1446–1474, <https://doi.org/10.1016/j.joule.2022.06.003>.
- [8] S. Sangsang Sasomwiyono, A. Fadlil, A.C. Subrata, Optimum solar energy harvesting system using artificial intelligence, *ETRI J.* (2022), <https://doi.org/10.4218/etrij.2022-0184>.
- [9] S. Shafian, G.E. Lee, H. Yu, J.-h. Jeong, K. Kim, High-efficiency vivid color CIGS solar cell employing nondestructive structural coloration, *Solar RRL* 6 (2022), 2100965, <https://doi.org/10.1002/solr.202100965>.
- [10] A.J.N. Oliveira, J.P. Teixeira, D. Ramos, P.A. Fernandes, P.M.P. Salomé, Exploiting the optical limits of thin-film solar cells: a review on light management strategies in Cu(In,Ga)Se₂, *Adv. Photonics Res* (2022), 2100190, <https://doi.org/10.1002/adpr.202100190>.
- [11] S. Lee, G.-Y. Yoo, B. Kim, M.K. Kim, C. Kim, S.Y. Park, H.C. Yoon, W. Kim, B.K. Min, Y.R. Do, RGB-colored Cu(In,Ga)(S,Se)₂ thin-film solar cells with minimal efficiency loss using narrow-bandwidth stopband nano-multilayered filters, *ACS Appl. Mater. Interfaces* 11 (2019) 9994–10003, <https://doi.org/10.1021/acsami.8b21853>.
- [12] C. Ji, Z. Zhang, T. Masuda, Y. Kudo, L.J. Guo, Vivid-colored silicon solar panels with high efficiency and non-iridescent appearance, *Nanoscale Horiz.* 4 (2019) 874–880, <https://doi.org/10.1039/C8NH00368H>.
- [13] D.H. Cho, W.J. Lee, M.E. Kim, B. Shin, Y.-D. Chung, Color tuning in Cu(In,Ga)Se₂ thin-film solar cells by controlling optical interference in transparent front layers, *Prog. Photovoltaics Res. Appl.* 28 (2020) 798–807, <https://doi.org/10.1002/ppp.3272>.
- [14] H.K. Raut, V.A. Ganesh, A.S. Nair, S. Ramakrishna, Anti-reflective coatings: a critical, in-depth review, *Energy Environ. Sci.* 4 (2011) 3779, <https://doi.org/10.1039/c1ee01297e>.
- [15] C.-E. Weng, B.-S. Chen, J.-J. Lin, Y.-L. Wu, C.-F. Yang, Comparison of measurement results of MgF₂-Nb₂O₅ distributed Bragg reflectors with different periods, *Mod. Phys. Lett. B* 36 (2022), <https://doi.org/10.1142/s0217984922500555>.
- [16] M. Mazur, D. Wojcieszak, J. Domaradzki, D. Kaczmarek, S. Song, F. Placido, TiO₂/SiO₂ multilayer as an antireflective and protective coating deposited by microwave assisted magnetron sputtering, *Opto-Electron. Rev.* 21 (2013) 233–238, <https://doi.org/10.2478/s11772-013-0085-7>.
- [17] Y. Luo, G. Chen, S. Chen, N. Ahmad, M. Azam, Z. Zheng, Z. Su, M. Cathelinaud, H. Ma, Z. Chen, P. Fan, X. Zhang, G. Liang, Carrier transport enhancement mechanism in highly efficient antimony selenide thin-film solar cell, *Adv. Funct. Mater.* 33 (2023), 2213941, <https://doi.org/10.1002/adfm.202213941>.
- [18] J. Lin, G. Chen, N. Ahmad, M. Ishaq, S. Chen, Z. Su, P. Fan, X. Zhang, Y. Zhang, G. Liang, Back contact interfacial modification mechanism in highly-efficient antimony selenide thin-film solar cells, *J. Energy Chem.* 80 (2023) 256–264, <https://www.sciencedirect.com/science/article/pii/S2095495623000761>.
- [19] S. Chen, Y. Fu, M. Ishaq, C. Li, D. Ren, Z. Su, X. Qiao, P. Fan, G. Liang, J. Tang, Carrier recombination suppression and transport enhancement enable high-performance self-powered broadband Sb₂Se₃ photodetectors, *InfoMat* 5 (2023), <https://doi.org/10.1002/inf2.12400>.
- [20] R. Tang, S. Chen, Z.H. Zheng, Z.H. Su, J.T. Luo, P. Fan, X.H. Zhang, J. Tang, G. X. Liang, Heterojunction annealing enabling record open-circuit voltage in antimony triselenide solar cells, *Adv. Mater.* 34 (2022), 2109078, <https://doi.org/10.1002/adma.202109078>.
- [21] P. Fan, Z. Xie, G. Liang, M. Ishaq, S. Chen, Z. Zheng, C. Yan, J. Huang, X. Hao, Y. Zhang, Z. Su, High-efficiency ultra-thin Cu₂ZnSnS₄ solar cells by double-pressure sputtering with spark plasma sintered quaternary target, *J. Energy Chem.* 61 (2021) 186–194, <https://www.sciencedirect.com/science/article/pii/S2095495621000553>.
- [22] G.-X. Liang, Y.-D. Luo, S. Chen, R. Tang, Z.-H. Zheng, X.-J. Li, X.-S. Liu, Y.-K. Liu, Y.-F. Li, X.-Y. Chen, Z.-H. Su, X.-H. Zhang, H.-L. Ma, P. Fan, Sputtered and selenized Sb₂Se₃ thin-film solar cells with open-circuit voltage exceeding 500 mV, *Nano Energy* 73 (2020), 104806, <https://www.sciencedirect.com/science/article/pii/S2211285520303633>.
- [23] D.-H. Cho, W.-J. Lee, M.E. Kim, K. Kim, J.H. Yun, Y.-D. Chung, Reactively sputtered Zn(O,S) buffer layers for controlling band alignment of Cu(In,Ga)Se₂ thin-film solar cell interface, *J. Alloys Compd.* 842 (2020), 155986, <https://doi.org/10.1016/j.jallcom.2020.155986>.
- [24] D.-H. Cho, W.-J. Lee, B. Shin, Y.-D. Chung, Analysis of vertical phase distribution in reactively sputtered zinc oxysulfide thin films, *Appl. Surf. Sci.* 486 (2019) 555–560, <https://doi.org/10.1016/j.apsusc.2019.04.200>.
- [25] D. Cho, W.J. Lee, Y.-D. Chung, *Color Device and Manufacturing Method of the Same*, vol. 10, 2021, 0116207. Korea.
- [26] W.-J. Lee, D.-H. Cho, J.-H. Wi, J.H. Yu, W.-J. Kim, C. Kang, S.J. Kang, Y.-D. Chung, Evolution of morphological and chemical properties at p-n junction of Cu(In,Ga)Se₂ solar cells with Zn(O,S) buffer layer as a function of KF postdeposition treatment time, *ACS Appl. Mater. Interfaces* 13 (2021) 48611–48621, <https://doi.org/10.1021/acsami.1c12636>.
- [27] J.H. Yu, D.-H. Cho, W.-J. Lee, W.-J. Kim, S.J. Kang, Y.-D. Chung, Application of quantum dot down-conversion layer in thin-film solar cells to increase short-wavelength spectral response, *ECS J. Solid State Sci. Technol.* 10 (2021), 055012, <https://doi.org/10.1149/2162-8777/abfb3>.
- [28] D.-H. Cho, S.-H. Hong, W.-J. Lee, J.Y. Kim, Y.-D. Chung, Colorful solar cells utilizing off-axis light diffraction via transparent nanograting structures, *Nano Energy* 80 (2021), 105550, <https://doi.org/10.1016/j.nanoen.2020.105550>.
- [29] D.-H. Cho, H.S. Jo, W.-J. Lee, T.-G. Kim, B. Shin, S.S. Yoon, Y.-D. Chung, Enhanced electrical conductivity of transparent electrode using metal microfiber networks for gridless thin-film solar cells, *Sol. Energy Mater. Sol. Cells* 200 (2019), 109998, <https://doi.org/10.1016/j.solmat.2019.109998>.
- [30] J.-H. Wi, W.S. Han, W.-J. Lee, D.-H. Cho, H.-J. Yu, C.-W. Kim, C. Jeong, J.H. Yun, C.-I. Kim, Y.-D. Chung, Spectral response of CuGaSe₂/Cu(In,Ga)Se₂ monolithic tandem solar cell with open-circuit voltage over 1 V, *IEEE J. Photovoltaics* 8 (2018) 840–848, <https://doi.org/10.1109/JPHOTOV.2018.2799168>.
- [31] W.-J. Lee, D.-H. Cho, J.M. Bae, M.E. Kim, J. Park, Y.-D. Chung, Ultrafast wavelength-dependent carrier dynamics related to metastable defects in Cu(In,Ga)Se₂ solar cells with chemically deposited Zn(O,S) buffer layer, *Nano Energy* 74 (2020), 104855, <https://doi.org/10.1016/j.nanoen.2020.104855>.
- [32] W.-J. Lee, D.-H. Cho, J.-H. Wi, H.-J. Yu, W.S. Han, J.M. Bae, J. Park, Y.-D. Chung, Ultrafast photocarrier dynamics at the p-n junction in Cu(In,Ga)Se₂ solar cell with various Zn(O,S) buffer layers measured by optical pump-terahertz probe spectroscopy, *ACS Appl. Energy Mater.* 1 (2018) 522–530, <https://doi.org/10.1021/acsaem.7b00127>.
- [33] W.J. Lee, H.J. Yu, J.H. Wi, D.H. Cho, W.S. Han, J. Yoo, Y. Yi, J.H. Song, Y. D. Chung, Behavior of photocarriers in the light-induced metastable state in the p-n heterojunction of a Cu(In,Ga)Se₂ solar cell with CBD-ZnS buffer layer, *ACS Appl. Mater. Interfaces* 8 (2016) 22151–22158, <https://doi.org/10.1021/acsami.6b05005>.
- [34] H. Cho, C.W. Joo, B.H. Kwon, C.M. Kang, S. Choi, J.W. Sin, Correlation between optimized thicknesses of capping layer and thin metal electrode for efficient top-emitting blue organic light-emitting diodes, *ETRI J.* (2022), <https://doi.org/10.4218/etrij.2022-0236>.
- [35] B.K. Meyer, A. Polity, B. Farangis, Y. He, D. Hasselkamp, T. Krämer, C. Wang, Structural properties and bandgap bowing of ZnO_{1-x}S_x thin films deposited by reactive sputtering, *Appl. Phys. Lett.* 85 (2004) 4929–4931, <https://doi.org/10.1063/1.1825053>.
- [36] L. Vegard, Die Konstitution der Mischkristalle und die Raumfüllung der Atome, *Z. Phys.* 5 (1921) 17–26, <https://doi.org/10.1007/BF01349680>.
- [37] B.K. Meyer, A. Polity, B. Farangis, Y. He, D. Hasselkamp, T. Krämer, C. Wang, U. Haboeck, A. Hoffmann, On the composition dependence of ZnO_{1-x}S_x, *Phys. Status Solidi C* 1 (2004) 694–697, <https://doi.org/10.1002/pssc.200304256>.
- [38] J.A. Van Vechten, T.K. Bergstresser, Electronic structures of semiconductor alloys, *Phys. Rev. B* 1 (1970) 3351–3358, <https://link.aps.org/doi/10.1103/PhysRevB.1.3351>.
- [39] C. Persson, C. Platzer-Björkman, J. Malmström, T. Törndahl, M. Edoff, Strong valence-band offset bowing of ZnO_{1-x}S_x enhances p-type nitrogen doping of ZnO-like alloys, *Phys. Rev. Lett.* 97 (2006), 146403, <https://link.aps.org/doi/10.1103/PhysRevLett.97.146403>.
- [40] M. Buffière, S. Harel, C. Guillot-Deudon, L. Arzel, N. Barreau, J. Kessler, Effect of the chemical composition of co-sputtered Zn(O,S) buffer layers on Cu(In,Ga)Se₂ solar cell performance, *Phys. Status Solidi A* 212 (2015) 282–290, <https://doi.org/10.1002/pssa.201431388>.
- [41] C.H. Frijters, P. Poort, A. Illiberi, Atmospheric spatial atomic layer deposition of Zn(O,S) buffer layer for Cu(In,Ga)Se₂ solar cells, *Sol. Energy Mater. Sol. Cells* 155 (2016) 356–361, <https://doi.org/10.1016/j.solmat.2016.06.016>.
- [42] J.R. Bakke, J.T. Tanskanen, C. Hägglund, T.A. Pakkanen, S.F. Bent, Growth characteristics, material properties, and optical properties of zinc oxysulfide films deposited by atomic layer deposition, *J. Vac. Sci. Technol. A* 30 (2012), 01A135, <https://doi.org/10.1116/1.3664758>.
- [43] Z. Jehl, M. Bouttemy, D. Lincot, J.F. Guillemoles, I. Gerard, A. Etcheberry, G. Voorwinden, M. Powalla, N. Naghavi, Insights on the influence of surface roughness on photovoltaic properties of state of the art copper indium gallium diselenide thin films solar cells, *J. Appl. Phys.* 111 (2012), 114509, <https://doi.org/10.1063/1.4721648>.
- [44] M. Bouttemy, P. Tran-Van, I. Gerard, T. Hildebrandt, A. Causier, J.L. Pelouard, G. Dagher, Z. Jehl, N. Naghavi, G. Voorwinden, B. Dimmler, M. Powalla, J. F. Guillemoles, D. Lincot, A. Etcheberry, Thinning of CIGS solar cells: Part I: chemical processing in acidic bromine solutions, *Thin Solid Films* 519 (2011) 7207–7211, <https://doi.org/10.1016/j.tsf.2010.12.219>.